PLEASE CITE THIS ARTICLE AS DOI: 10.1063/5.0170650

Ryan P. Collanton, Christopher J. Ellison, and Kevin D. Dorfman^{a)} Department of Chemical Engineering and Materials Science, University of Minnesota-Twin Cities, 421 Washington Ave. SE, Minneapolis, MN 55455, USA

(Dated: 11 October 2023)

Block copolymers at homopolymer interfaces are poised to play a critical role in the compatibilization of mixed plastic waste, an area of growing importance as the rate of plastic accumulation rapidly increases. Using molecular dynamics simulations of Kremer–Grest polymer chains, we have investigated how the number of blocks and block degree of polymerization in a linear multiblock copolymer impacts the interface thermodynamics of strongly segregated homopolymer blends, which is key to effective compatibilization. The second virial coefficient reveals that interface thermodynamics are more sensitive to block degree of polymerization than to the number of blocks. Moreover, we identify a strong correlation between surface pressure (reduction of interfacial tension) and the spatial uniformity of block junctions on the interface, yielding a morphological framework for interpreting the role of compatibilizer architecture (number of blocks) and block degree of polymerization. These results imply that, especially at high interfacial loading, the choice of architecture of a linear multiblock copolymer compatibilizing surfactant does not greatly affect the modification of interfacial tension.

a) Electronic mail: dorfman@umn.edu

PLEASE CITE THIS ARTICLE AS DOI: 10.1063/5.0170650

I. INTRODUCTION

Questions about the properties and design of blended polymer materials are especially relevant in the modern world. Polymer materials are produced at an annually growing rate, and plastic waste streams are increasingly heterogeneous in composition.^{1–5} However, chemically distinct polymers are typically immiscible due to differences in monomer chemistry which engender (sometimes small) interaction penalties that are amplified by the significant length of polymer chains, as quantified by Flory–Huggins solution theory.⁶ These unfavorable interactions drive phase separation in blends of common and ostensibly similar polymers, such as polyethylene and isotactic polypropylene.⁷ Such polymeric blends exhibit physical properties that, due to the presence of phase-separated domains, vary on undesirably long length scales.^{8,9} Additionally, weak or nearly non-existent adhesion between layers at domain interfaces lead to facile layer separation and poor macroscopic mechanical properties such as early failure and low yield stress.^{10,11} Addressing these issues is critical for advancing recycling of mixed plastic waste.

This study focuses on understanding and mitigating the driving force for the formation of large domains in immiscible polymer blends through the addition of linear multiblock copolymer compatibilizers. Block copolymers are known to have an emulsifying effect in blends of thermodynamically immiscible homopolymers, analogous to the role of small-molecule surfactants in immiscible liquids. ^{12–15} They aggregate at the homopolymer interface, where they exclude homopolymers and introduce an attractive force across the interface through block junction bonds, thereby reducing interfacial tension. ^{16,17} This effect in turn reduces the penalty for material homogeneity by allowing a larger interfacial area per unit volume, effectively reducing domain size. The degree of domain size reduction corresponds, to a first approximation, with the extent to which the block copolymers reduce the interfacial tension, although in practice non-equilibrium factors such as processing also play a role. ^{18–20}

There is a large body of prior work investigating the surfactant-like effects of block copolymers at homopolymer interfaces.^{8,9,12–17,21–29} However, theoretical investigations have largely focused on the emulsifying effects of diblock copolymers due to their close analogy with small molecule surfactants, with limited exploration of the role of block copolymer architecture.^{12–16,21–23,25,26,30} Diblock copolymers constitute the simplest possible architecture of a copolymer surfactant, with only one free parameter in the commonly studied

PLEASE CITE THIS ARTICLE AS DOI: 10.1063/5.0170650

case of a compositionally symmetric diblock, leaving little room for tuning and optimizing material properties. Given recent outstanding experimental success demonstrating linear multiblock copolymers as promising compatibilizer additives, 8,9,29,31 it is critical to supplement previous theoretical work by considering the role of architecture. To vary architecture of a linear multiblock copolymer, we change the number or chemical identities of the blocks. The large space of possible architectures can be strategically navigated to answer specific questions, such as by varying monomer sequence along a fixed-length copolymer chain or by linking together copolymer chains. In this study, to vary the architecture of a linear multiblock copolymer, we change the number of blocks and alternate monomer type (B, A, B. ...). By conceptualizing linear multiblock copolymers as multimers of diblock copolymers, we disentangle the impact of design parameters (number of blocks, block degree of polymerization, and copolymer interfacial loading) on interface thermodynamics. We also identify a morphological correlation between interface thermodynamics and junction clustering, and describe a framework for understanding the effect of block copolymer design on interfacial tension.

II. **METHODOLOGY**

Α. Polymer Model

In this work, we model polymers as coarse-grained Kremer-Grest bead-spring chains. 32,33 Specifically, pairwise interactions between all beads, bonded and nonbonded, are modeled with the Lennard-Jones (LJ) potential truncated to the repulsive component. This potential, also known as the Weeks-Chandler-Andersen (WCA) potential,³⁴ is given by

$$u_{ij}^{\text{WCA}}(r) = \begin{cases} 4\epsilon_{ij} \left[\left(\frac{\sigma}{r} \right)^{12} - \left(\frac{\sigma}{r} \right)^{6} \right] + \epsilon_{ij} & r < 2^{1/6}\sigma \\ 0 & r \ge 2^{1/6}\sigma \end{cases}$$
(1)

where the i and j indices correspond to bead types (i.e., A and B monomers), ϵ_{ij} is the repulsion strength between monomer i and j, and σ is the LJ length scale. The LJ energy parameters are $\epsilon_{AA} = \epsilon_{BB} = \epsilon$, and $\epsilon_{AB} = 50\epsilon$, putting the system firmly in the strong segregation regime (see the Supplementary Material). Bonds between neighbor beads on

PLEASE CITE THIS ARTICLE AS DOI: 10.1063/5.0170650

the chains are enforced using the finitely extensible nonlinear elastic (FENE) potential,

$$u^{\text{FENE}}(r) = -\frac{1}{2}kr_0^2 \ln \left[1 - \left(\frac{r}{r_0}\right)^2\right]$$
 (2)

where k is the spring constant and r_0 sets the maximum bond length. The parameters of the FENE potential are consistent with literature values known to prevent bond crossing $(r_0 = 1.5\sigma, k = 30\epsilon/\sigma^2)$. The fundamental unit of time is $\tau = \sigma(m/\epsilon)^{1/2}$, where m is the mass of the A and B beads. Energies here and hereafter are reported in units of $k_B T$, where k_B is Boltzmann's constant and T is the absolute temperature.

B. Structure Generation

Systems are configured as three homopolymer rich regions separated by two interfaces in the yz-plane with copolymers adsorbed to the interfaces. The simulation box size is determined by setting an average density of $\rho=0.85\sigma^{-3}$ and using box lengths $L_y=L_z=aL_x$ with an aspect ratio a=0.544 to ensure the interfaces are separated enough that the copolymer brushes do not interact within or across box images. Individual polymer chain conformations are generated using a modified version of the Monte Carlo random-walk procedure from Kremer and Grest.³² This procedure consists of performing a 3D Brownian random walk augmented with an acceptance condition to prevent unrealistic backfolding. At each step i, the distance between bead (i) and bead (i-2) is required to be larger than some threshold; a detailed explanation of this procedure is available in Ref. 32. For block copolymers, blocks are generated independently and then linked together with the same two-step distance condition.

Each homopolymer chain is then placed at random in a region of the simulation box according to its type. The systems are initialized in the phase-separated state to accelerate equilibration. A small study was done to confirm that phase separation of the A and B chains does occur spontaneously from an initially homogeneous configuration at low to modest interaction strengths, providing confidence that initially phase-separated states are not kinetically trapped (see the Supplementary Material).

Copolymer random-walk chains are placed at the two interfaces between the A and B regions, with no particular initial orientation. Chains are thus initialized with a conformation that does not account for the thermodynamic interactions of homopolymers with copolymer

PLEASE CITE THIS ARTICLE AS DOI: 10.1063/5.0170650

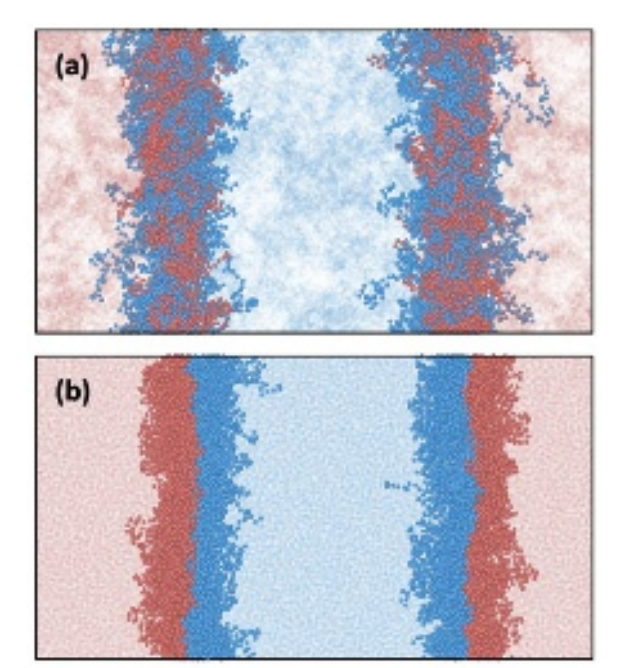


FIG. 1. A ternary blend of homopolymers with triblock copolymers of $N_{\rm b}=32$ and $M_{\rm CP}=128$ at (a) the random initial state and (b) after a production run of $5\times 10^4\tau$. A beads are red and B beads are blue. Copolymer beads are opaque while homopolymer beads are semi-transparent.

blocks, such that some B blocks might traverse through an A homopolymer region and vice versa, and junctions are not located at the interface. A representative example of such a randomly generated structure is shown in Fig. 1a.

C. Simulation Protocol

The initial structure is first relaxed to address aphysical overlaps inevitably resulting from the random initialization procedure. First, a short simulation replacing Eq. (1) with a soft Gaussian pairwise potential given by $u(r) = C \exp(-\frac{1}{2}(r/\sigma)^2)$ is performed, where the prefactor C is continuously ramped up from C = 1 to C = 120, slowly easing overlapping beads off of each other.³² Next, the full pairwise LJ potential is applied and a short simulation is performed with a capped-displacement integrator that effectively cools the system and relaxes all overlaps with very few iterations ($<1 \times 10^5$ steps at $\Delta t = 0.005\tau$).

Following relaxation, the system is then equilibrated to remove artifacts of the initialization procedure, such as large density fluctuations and random conformations of copolymers at the interface, and reach a dynamic equilibrium. Here, the system is evolved using

PLEASE CITE THIS ARTICLE AS DOI: 10.1063/5.0170650

Langevin dynamics in the NVT ensemble using a time step of $\Delta t = 0.005\tau$. The temperature is held at $k_{\rm B}T = \epsilon$ through coupling to a thermal reservoir with a drag coefficient $\Gamma_d = 1.0$. Stable macroscopic properties are necessary but not sufficient for equilibration, as chain deformations on intermediate length scales are known to relax on longer time scales. Following the analysis of Auhl et~al., ³⁶ we compute internal segment length distributions, an example of which is given in Fig. 2, confirming that they quantitatively match the profile of an equilibrated melt. Homopolymers and copolymers are treated separately in this analysis; the interface induces stretching of the copolymers that would be non-equilibrium for bulk homopolymer. All systems fully equilibrate within 4×10^7 steps.

The final production run is identical to the equilibration step with one important exception: center of mass momentum is zeroed out every 50 iterations to facilitate better collection of accurate spatial data. The systems are simulated for 1×10^7 time steps. The equilibration and production steps could have been performed using the NP_xAT ensemble, which fixes the interfacial area and the diagonal element of the stress tensor normal to the interface. A brief investigation revealed this approach produces results quantitatively indistinguishable from NVT ensemble calculations (see Fig. S1). Note that the NPT ensemble is incompatible with the Kirkwood-Buff method for computing the interfacial tension, which relies on differences between diagonal elements of the stress tensor (see the next section). All molecular dynamics simulations were performed with the open-source HOOMD-blue software package. 37,38 Images of an example initial structure with Monte-Carlo random-walk chains and the same system after the full simulation pipeline are given in Fig. 1.

D. Computing Interfacial Tension

The ensemble average interfacial tension is computed following the description of Kirkwood and Buff, 39,40

$$\langle \gamma \rangle = \frac{L_{\rm x}}{2} \langle P_{\rm N} - P_{\rm T} \rangle \tag{3}$$

where $P_{\rm N}=P_{\rm xx}$ and $P_{\rm T}=(P_{\rm yy}+P_{\rm zz})/2$ are the components of the global pressure tensor normal and tangential to the interface, respectively. Averages were computed over independent samples, determined using an estimate of the autocorrelation time of the interfacial tension. The exact details of the statistical treatment are in the Supplementary Material.

PLEASE CITE THIS ARTICLE AS DOI: 10.1063/5.0170650

2 homopolymer 2 diblock copolymer 1 triblock copolymer 2 pentablock copolymer 1 notation in the second second

FIG. 2. Segment length per bead as a function of segment degree of polymerization, $\langle R^2(N)\rangle/N$. Gray curves are replica results, and blue curves are their average. The approximate monotonicity and leveling off of the homopolymer distributions confirm no non-equilibrium internal stretching deformations.³⁶ The copolymer distributions exhibit sharp increases indicating stretching and decreases corresponding with midblock loops. Data shown are for blends with 128 junctions per interface and $N_{\rm b}=32$.

E. Gaussian smeared density of a point cloud

To analyze the spatial uniformity of junctions at the interface, we project their location onto the Gibbs dividing surface and construct a two-dimensional point cloud. The Gaussian smear transforms this point cloud into a continuous density function. It is strictly a

PLEASE CITE THIS ARTICLE AS DOI: 10.1063/5.0170650

convolution, and can be expressed as the sum of a set of Gaussian distributions with width λ centered at each point in the cloud. In two dimensions, the Gaussian smear continuous density profile is

 $\rho_c(\mathbf{r}) = \sum_i \frac{1}{2\pi\lambda^2} \exp\left(-\frac{\|\mathbf{r} - \mathbf{r}_i\|^2}{2\lambda^2}\right)$ (4)

where the sum is over the points in the point cloud. When computing $\|\mathbf{r} - \mathbf{r}_i\|$, care must be taken to account for periodic boundary conditions. Furthermore, the distribution width λ is a tunable parameter of the convolution, with larger widths corresponding to greater smearing of the point cloud. We swept the value of the width parameter and found that, except for large $(\lambda > 8)$ or small $(\lambda < 1)$ values, it did not qualitatively impact our findings. Within this range and for the purpose of extracting qualitative understanding of the system, this method is effectively parameter-free. An intermediate value ($\lambda = 3.5$) was chosen that is large enough to adequately smear the point cloud while small enough not to wash out detail in the point cloud. The variance of the continuous density profile is calculated as

$$\sigma_{\rho}^{2} = \frac{1}{A} \int_{\Sigma} d\mathbf{r} \ \rho_{c}(\mathbf{r})^{2} - \langle \rho \rangle^{2}$$
 (5)

where Σ is the two-dimensional region constituting the interface and A is the area of this region. After discretizing, the equivalent form is

$$\sigma_{\rho}^{2} = \frac{1}{n} \sum_{i=1}^{n} \rho_{i}^{2} - \langle \rho \rangle^{2} \tag{6}$$

where n is the number of bins, $\rho_i = \rho_c(\mathbf{r}_j)$ is the smeared density in bin j, and \mathbf{r}_j is the center of bin j. Notably, the binned value ρ_i depends only on bin location and not on bin size.

Study Design $\mathbf{F}.$

The number $(M_A = M_B = M = 1024)$ and degree of polymerization $(N_h = 64)$ of A and B homopolymers are fixed. Linear multiblock copolymers are constructed with 2, 3, or 5 blocks of alternating monomer type (BA, BAB, or BABAB). During the simulation time, block copolymers stay on the interface due to strong repulsion and significant block degrees of polymerization, preventing complicating effects such as micellization and bulk solubilization. These are experimentally important factors that compete with localization of

PLEASE CITE THIS ARTICLE AS DOI: 10.1063/5.0170650

the block copolymers to the interface. Rare simulation examples that exhibited micellization were excluded from the dataset to focus the results solely on the case of a fixed surface concentration of block polymer.

Comparisons between systems of differing copolymer architecture are made by treating triblock copolymers as dimers of diblocks, and pentablocks treated as dimers of triblocks, in both cases fixing the number of parent diblocks. A base degree of polymerization $N_{\rm b}$ sets the degree of polymerization of the copolymer endblocks, and with the dimerization interpretation all midblocks are twice as long. Systems of the same base degree of polymerization with $M_{\rm CP}=X$ diblocks, $M_{\rm CP}=X/2$ triblocks, and $M_{\rm CP}=X/4$ pentablocks, where $M_{\rm CP}$ is the number of copolymers, are treated as a slice of the data where only the number of blocks in, or equivalently the architecture of, the copolymer is varied. Architectural variations thus preserve the total number of copolymer beads and the number of block junctions, but vary the total number of copolymers.

TABLE I. The copolymer terminal/base block length $(N_{\rm b})$, copolymer block degrees of polymerization $(N_{\rm CP})$, number of copolymers $(M_{\rm CP})$, and number of junctions per interface for each ternary polymer blends included in this study. Copolymer types are BA, BAB, and BABAB. Each system has M=1024 homopolymers of degree of polymerization $N_{\rm h}=64$. Copolymer volume fraction is constant at fixed base length and fixed number of junctions per interface. Systems are contrasted across varying architecture for fixed number of junctions per interface and fixed $N_{\rm b}$.

$N_{ m b}$	$N_{ m CP}$	M_{CP}	jxn/interface	
16	(16, 16)	32 - 384	16 - 192	
16	(16, 32, 16)	16 - 192	16 - 192	
16	(16, 32, 32, 32, 16)	8 - 96	16 - 192	
32	(32, 32)	32 - 384	16 - 192	
32	(32, 64, 32)	16 - 192	16 - 192	
32	(32, 64, 64, 64, 32)	8 - 96	16 - 192	
64	(64, 64)	32 - 384	16 - 192	
64	(64, 128, 64)	16 - 192	16 - 192	
64	(64, 128, 128, 128, 64)	8 - 96	16 - 192	

rubilishing Chemical Phy

This is the author's peer reviewed, accepted manuscript. However, the online version of record will be different from this version once it has been copyedited and typeset

PLEASE CITE THIS ARTICLE AS DOI: 10.1063/5.0170650

(a)

(b) $N_b = 2N_b \cdots 2N_b N_b$ $N_b = 16 \times \text{diblock}$ $N_b = 32 \quad \triangle \text{ triblock}$ $N_b = 64 \quad \bigcirc \text{pentablock}$

FIG. 3. (a) Schematic indicating the dimerization of two diblock copolymers to form a single triblock copolymer, preserving copolymer volume fraction, the number of copolymer beads, and the number of block junctions per interface, but changing the number of copolymer molecules. (b) Framework for the construction of linear multiblock copolymers, with corresponding colors and markers used in figures throughout this paper.

Considering this framework, which is depicted schematically in Fig. 3 and explicitly in Table I, the key variables swept in this study are the copolymer endblock base degree of polymerization $N_{\rm b}$, the total number of block junctions, and the number of blocks in the linear block copolymer. The number of copolymers is implicit on the number of blocks and the total number of block junctions.

III. INTERFACIAL TENSION OF TERNARY BLENDS

We first present interfacial tension data for phase-separated ternary blends of A and B homopolymers with alternating A/B linear multiblock copolymers. Figure 4 displays the surface pressure $\Pi = \gamma_0 - \gamma$ as a function of copolymer surface density (Fig. 4a) and block junction surface density (Fig. 4b), where γ_0 is the interfacial tension of the bare homopolymer-homopolymer blend and γ is the interfacial tension of the ternary system.

PLEASE CITE THIS ARTICLE AS DOI: 10.1063/5.0170650

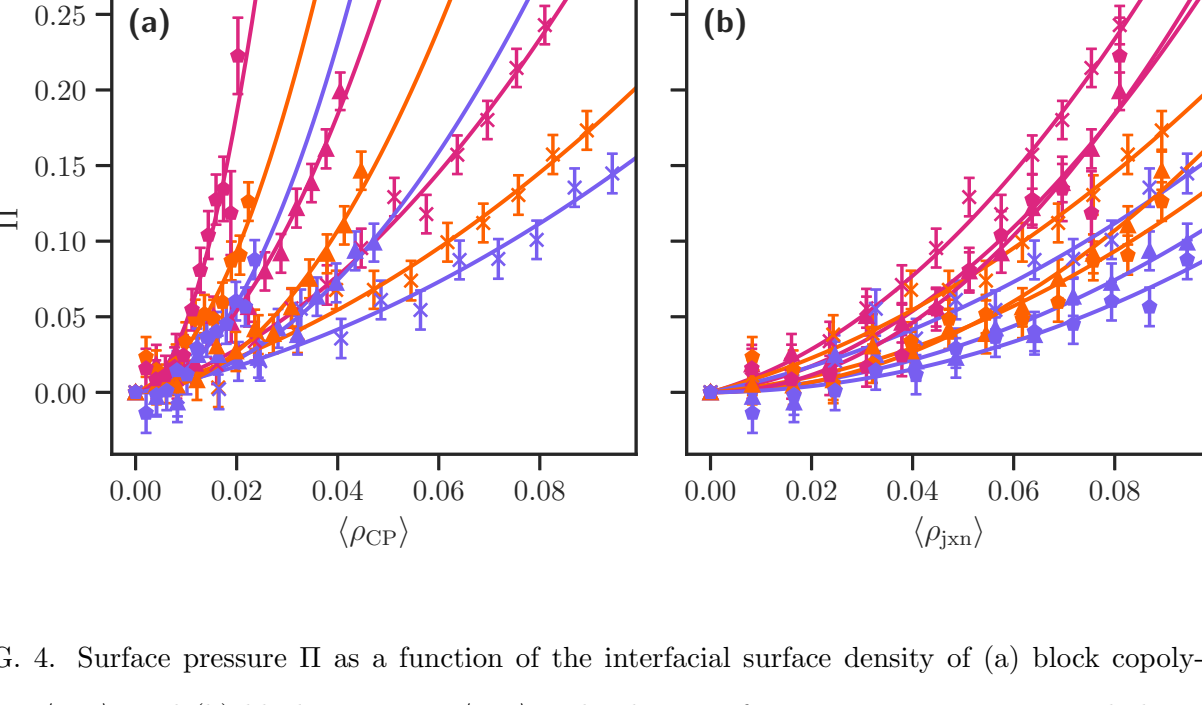


FIG. 4. Surface pressure Π as a function of the interfacial surface density of (a) block copolymers, $\langle \rho_{\rm CP} \rangle$, and (b) block junctions, $\langle \rho_{\rm jxn} \rangle$. The density of junctions is a more natural choice of dependent variable as it fixes weight fraction and better correlates with surface pressure across systems. Lines are fits of Eq. (7), with fit parameters given in Table II. As described in Fig. 3b, colors indicate block lengths $N_{\rm b}=16$ (purple), $N_{\rm b}=32$ (orange), and $N_{\rm b}=64$ (red), and symbols indicate diblock (cross), triblock (triangle), and pentablock (pentagon) copolymer architectures. Error bars are two times the standard error of the mean (see the Supplementary Material).

Adsorption data for each copolymer are fit to a virial equation of state truncated to second order,

$$\frac{\Pi}{k_{\rm B}T\langle\rho\rangle} = A + B\langle\rho\rangle \tag{7}$$

where A and B are the first and second virial coefficients. As expected, surface pressure increases (interfacial tension decreases) with increasing surface density. From Fig. 4a, copolymers with a larger number of blocks exert a higher surface pressure at fixed copolymer surface density. However, in this presentation of the data, the systems vastly differ in weight fraction, and do not isolate the effect of architecture. The surface density of junctions better correlates surface pressure data, demonstrated by the relatively greater similarity of curves in Fig. 4b. This increased similarity is consistent with the fact that copolymers function as multisite adsorbents and reinforces the idea that junctions, not entire molecules, are the

PLEASE CITE THIS ARTICLE AS DOI: 10.1063/5.0170650

effective adsorbents to the interface. Moving forward, we will use the notation $\langle \rho \rangle$ to denote the average areal junction density, equal to the number of junctions divided by the interfacial area.

Focusing on Fig. 4b, two other features of the data stand out. First, increasing block degree of polymerization $N_{\rm b}$ tends to increase surface pressure. Second, at fixed $N_{\rm b}$ diblock copolymers exert a marginally higher surface pressure than linear multiblock copolymers. Importantly, surface pressure is markedly more sensitive to block degree of polymerization than to architecture. This is consistent with the calculations of Noolandi,⁴¹ which demonstrate that for multiblock copolymers to be effective as surfactants, their blocks must be long enough to extend beyond the original homopolymer interface into the homopolymer bulk region.

Table II contains the first and second virial coefficients obtained by fits of Eq. (7) to Fig. 4, constrained to be positive, with either the density of copolymers $\langle \rho_{\text{CP}} \rangle$ or density of junctions $\langle \rho_{\text{jxn}} \rangle$ as the dependent variable. Notably, the second virial coefficients for a given value of N_{b} are much closer in magnitude across all systems when junction density is the dependent variable. Likewise, systems with diblock copolymers exhibit first virial

TABLE II. Virial coefficients for ternary blends resulting from fits of Eq. (7) to the thermodynamic data of surface pressure versus average copolymer density and junction density in Fig. 4.

		copolymer		junction	
$N_{ m b}$	Num. Blocks	A	В	A	В
16	2	0.68	8.9	0.68	8.9
16	3	0.28	39	0.14	9.7
16	5	0.11	141	0.028	8.8
32	2	0.91	11	0.91	11
32	3	0.00	67	0.00	17
32	5	1.23	170	0.31	11
64	2	0.93	25	0.93	25
64	3	0.79	95	0.39	24
64	5	0.00	460	0.00	29

PLEASE CITE THIS ARTICLE AS DOI: 10.1063/5.0170650

coefficients closer to unity, suggesting approximate two-dimensional ideal gas behavior of the junctions at low density, consistent with the results of Mysona $et\ al.^{30}$ However, multiblock copolymer junctions are correlated due to finite midblock length, and thus deviate from ideal gas behavior at low density, as indicated by lower first virial coefficients when compared to diblock copolymers. With junction density as the dependent variable, the second virial coefficient varies more with respect to $N_{\rm b}$ than the number of blocks.

Further information about the role of architecture can be gleaned by normalizing the surface pressure of the pentablock and triblock systems to the surface pressure of the matching diblock system (the one at identical base block degree of polymerization and junction density), as presented in Fig. 5. This normalization effectively removes the role of block degree of polymerization. The low density region, where interfacial tension is reduced by less than 5%, is excluded from the figure. At large junction density, the normalized surface pressures collapse to within measurement error. The positive trend in normalized surface pressure reveals that the effect of multiblock copolymers approaches that of diblock copolymers as junction density increases.

The key takeaway from these results is that, if surface density of junctions is fixed, the effect of block degree of polymerization on surface pressure is much more significant than that of architecture. To the extent that the number of blocks in a linear multiblock copolymer does play a role, this role decreases as surface density of junctions increases. Thus, in the practically relevant region where the interfacial tension is meaningfully decreased, the impact of architecture can, to a first approximation, be ignored. Controlling interfacial loading of the compatibilizer is thus critical to controlling performance, and will require different blending fractions depending on the effects of architecture on bulk solubility and micellization.

IV. SPATIAL UNIFORMITY OF JUNCTIONS ON THE INTERFACE

It is clear from the above results that the surface pressure is impacted to a greater degree by copolymer block degree of polymerization than by architecture. Nonetheless, diblock copolymers exert a greater surface pressure than linear multiblock copolymers. In what follows, we leverage structural features of block copolymers at the interface to construct a morphological interpretation of this architecture-related effect. This analysis leverages the

PLEASE CITE THIS ARTICLE AS DOI: 10.1063/5.0170650

1.25 1.00 0.750.500.250.00 -0.250.04 0.06 0.08 $\langle \rho \rangle$

FIG. 5. Surface pressure relative to that of the matching diblock system. Large error at low $\langle \rho \rangle$ is due to magnification of error in the vanishing denominator, $\Pi_{DB} \to 0$. In the higher surface density region of interest, the relative surface pressure trends towards unity as $\Pi \to \Pi_{DB}$. As described in Fig. 3b, colors indicate block lengths $N_{\rm b}=16$ (purple), $N_{\rm b}=32$ (orange), and $N_{\rm b}=64$ (red), and symbols indicate diblock (cross), triblock (triangle), and pentablock (pentagon) copolymer architectures. Error bars are two times the standard error of the mean (see the Supplementary Material).

wealth of microstructural information available from molecular dynamics simulations, which is not experimentally available, to complement the experimentally accessible interfacial tension data presented above.

Diblock and multiblock copolymers fundamentally differ in their conformations at the interface. The most immediate indication of this fact is in Fig. 2; midblocks must turn around to accommodate two ends on the interface, corresponding with sharp increases followed by decreases in internal segment end-to-end distances as a function of their contour length. Further illustrating this point, Fig. 6 shows the average end-to-end distances per bead for block copolymer segments within a single block starting at the block junction. Per-bead end-to-end distances increase along the segment, but midblocks start to turn around near the halfway point. Both midblocks and endblocks exhibit significantly higher end-to-end distances than equilibrium homopolymers which is a result of copolymer chains stretching

PLEASE CITE THIS ARTICLE AS DOI: 10.1063/5.0170650

Publishing Chemical Phys

FIG. 6. Average squared end-to-end distance per bead for endblock (blue) and midblock (red) segments starting at block junctions in (a) diblock, (b) triblock, and (c) pentablock copolymers. Equilibrium homopolymer curves (black) are included for comparison. Data shown are for blends with 128 junctions per interface and $N_{\rm b}=32$.

away from the interface.

Recalling the interpretation of multiblock copolymers as linked diblock copolymers, these midblock linkages mechanically couple junctions to each other. This constrains the freedom of multiblock junctions to move about the interface independently of each other, increasing junction clustering and effectively reduce the area occupied per junction relative to diblock junctions. Motivated by the strong dependence of surface pressure on average junction density in Fig. 4b, we examine local junction density fluctuations and, equivalently, the uniformity of junction spacing on the interface. First, we construct two-dimensional point clouds consisting of the projection of junction positions onto the Gibbs dividing surface; examples are given in Fig. 7a. To the naked (squinted) eye, the junctions of multiblock copolymers appear more clustered, while those of the diblock copolymers seem more evenly spaced. To quantitatively assess the evenness of junction density profiles and contrast them with the thermodynamic results of Figs. 4 and 5, we proceed with an approach utilizing Gaussian smearing (see the Methods section). We chose this method because it is sensitive to subtle differences in point clustering. Furthermore, it enables ensemble averaging of junction density that preserves density variance, whereas ensemble averaging over junction

PLEASE CITE THIS ARTICLE AS DOI: 10.1063/5.0170650

(a) 20 0.10 - 0.08 0 Š **-** 0.04 -20**(b)** 20 0.10 **-** 0.08 0 Š **-** 0.04 -20-200 20 -200 20 xx

FIG. 7. Point cloud (left) and Gaussian blurred density (right) of locations of junctions of (a) diblock copolymers and (b) triblock copolymers on the interface at the final frame of the production simulation. The triblock junctions appear clustered in pairs and exhibit higher peak density and density variation. Data shown are for blends with 128 junctions per interface and $N_{\rm b}=32..$

locations would homogenize the density. Examples of the transformation from point clouds to continuous density profiles are given in Fig. 7b.

The variance of the junction density relative to a reference state is a measure of the uniformity of junction spacing, with lower variance corresponding to a higher uniformity, and vice versa. To compute this quantity, we perform a Gaussian smear (blur) of the point cloud, discretize it, and then take the variance of the binned density values (σ_{ρ}^2) .⁴² We then

PLEASE CITE THIS ARTICLE AS DOI: 10.1063/5.0170650

compare this density variance with that of a reference two-dimensional system of WCA particles. We refer to this final quantity as the relative variance $\tilde{\sigma}_{\rho}^2 = (\sigma_{\rho}/\sigma_{\rho}^{\text{WCA}})^2$, and its inverse square root $1/\tilde{\sigma}_{\rho}$ as the "uniformity", which increases as junctions are spaced more uniformly on the interface.

The square root of the variance relative to that of the two-dimensional WCA fluid is given in Fig. 8a. At fixed average junction density, the density variance increases with increasing number of blocks, which is consistent with the fact that coupling junctions with midblocks reduces their ability to move independently of each other. The density variance also decreases with increasing block degree of polymerization. Because this is especially the case for multiblock copolymers, this decrease in density variance also supports the intuition that lengthening midblocks loosens the mechanical coupling between junctions.

At low junction densities, the relative density variance of diblock systems is nearly unity, almost exactly matching that of the reference WCA fluid, while multiblock systems display amplified relative variance. As junction density increases, the relative variance decreases, demonstrating that the effective range of repulsive interactions between junctions is larger than that of the corresponding 2D WCA fluid. Mechanistically, this effect is likely connected to steric interactions of the chains hanging off the junctions. This interpretation is further supported by the observation that the largest block degrees of polymerization consistently exhibit greater uniformity than the reference (relative variance less than unity).

To probe the connection between these spatial ideas and interface thermodynamics and arrive at the key conclusion of this paper, surface pressure is plotted against the junction uniformity (the inverse square root of relative variance) in Fig. 8b. The data collapse, depicting a clear correlation between the uniformity of copolymer junctions on the interface and the reduction of interfacial tension. This correlation can be rationalized by considering the mechanism of a block copolymer surfactant. The copolymer acts to exclude homopolymer from the interface, thereby reducing the unfavorable interactions and further countering them with bonded interactions across the interface from block junctions. As junctions cluster and chains stretch away from the interface, the interfacial area of excluded homopolymer per junction decreases, tipping the balance of forces and thus reducing the impact per copolymer on interfacial tension. The collapse of the data in Fig. 8b is relatively tight, but might be improved with a better choice of reference system or adjusting the density smearing technique. Two additional analyses of interfacial coverage that qualitatively support these connections

PLEASE CITE THIS ARTICLE AS DOI: 10.1063/5.0170650

(a) • 0.01 1.4 1.2 $\tilde{\sigma}_{\rho}$ 1.0 0.8 0.60.04 0.06 0.00 0.02 0.08 $\langle \rho \rangle$ 0.25 (b) 0.200.15 \square 0.10 0.05 0.00 0.8 1.2 1.0 1.4 1.6 uniformity $(1/\tilde{\sigma}_o)$

FIG. 8. (a) The variance of smeared junction density relative to a reference as a function of the average density. The inset gives the square root of the density variance of the reference twodimensional WCA fluid, $\sigma_{\rho}^{\text{WCA}}$. (b) Surface pressure versus junction uniformity, the inverse square root of relative variance, with a clear and strong positive correlation between uniformity and surface pressure.

are provided in the Supplementary Material.

Ultimately, understanding that the uniformity of junction spacing largely captures changes in surface pressure leads to an intuitive framework for predicting the role of architecture in reducing interfacial tension. Generally, changes that increase the uniformity of junction spacing will increase the surface pressure, such as increasing side chain steric repulsion, lengthening midblocks to reduce physical constraints, and cutting mechanical ties

PLEASE CITE THIS ARTICLE AS DOI: 10.1063/5.0170650

between junctions. We expect this framework will be consistent with architectures that would further enforce uniform junction spacing, such as star or bottlebrush copolymers, but a definitive test of this theory will require additional investigation.

V. CONCLUDING REMARKS

Interface thermodynamics are an important piece of the compatibilizer engineering problem. Previous works, both theoretical and experimental, have explored how diblock copolymer parameters impact the emulsification of immiscible homopolymers. Those works show that surface pressure increases (interfacial tension is reduced) with increasing block degree of polymerization and copolymer volume fraction. This work considers the role of block copolymer architecture in the context of linear multiblock copolymers and provides a morphological interpretation of the results, enabling a spatially intuitive way to think about the modification of interface thermodynamics by block copolymers. In essence, uniform spacing of adsorbents on the interface strongly correlates with reduction of interfacial tension. This information, coupled with considerations of transport, solubility, and micellization, should guide decisions about architecture when approaching compatibilizer design problems.

These results are naturally limited by the scope of this study. We focused explicitly on linear multiblock copolymers, and though we believe the correlation of surface pressure with junction spatial uniformity should extend to more complex architectures such as bottlebrush or miktoarm polymers, additional investigation would be necessary to confirm this hypothesis. Furthermore, the system in this study is a hypothetical lamellar-like system designed to isolate the interfacial thermodynamics and adsorbent spatial arrangement from complicating effects that might arise in a macroscopic system with polymer droplets, such as interfacial curvature and droplet population dynamics. Finally, this study focused on strongly segregated systems, with block copolymers that do not leave the interface, to cleanly extract information about their impact at the interface. However, phenomena such as micellization, bulk solubilization, or transport of block copolymers to and from the interface could complicate the results at lower segregation strengths, higher concentrations, or higher block degrees of polymerization. We highlight all of these as important routes for future investigation.

It is worth noting there are significant opportunities for corresponding experiments. While some interfacial tension measurements have been performed for block copolymers with dif-

ferent architectures and compositions. 17,43,44 a carefully designed model system offering synthetic access to a host of well-defined linear multiblock copolymer architectures with thermal properties suitable for standard surface tension measurement protocols would be powerful. Such experiments could also consider transport and micellization effects, practical issues that are not captured in these simulations.

SUPPLEMENTARY MATERIAL

The supplementary material contains details of the statistical treatment, ensemble choice, additional data, and two additional analyses to support the results of the main text.

ACKNOWLEDGMENTS

We thank Jeffrey L. Self, Gabriela Diaz, David C. Morse, and Frank S. Bates for valuable discussion. The authors acknowledge our principal funding source, the National Science Foundation Center for Sustainable Polymers at the University of Minnesota, which is a National Science Foundation supported Center for Chemical Innovation (CHE-1901635). Acknowledgement is made to the donors of the American Chemical Society Petroleum Research Fund for partial support of this research. The Minnesota Supercomputing Institute at the University of Minnesota provided computational resources used for this study.

AUTHOR DECLARATIONS

Conflict of Interest

The authors have no conflicts to disclose.

Author Contributions

Ryan P. Collanton conceptualization (equal); formal analysis (lead); investigation (lead); methodology (lead); software (lead); writing - original draft (lead); writing - review and editing (lead). Christopher J. Ellison conceptualization (supporting); writing - review and editing (supporting). Kevin D. Dorfman conceptualization (equal); methodology

PLEASE CITE THIS ARTICLE AS DOI: 10.1063/5.0170650

(supporting); supervision (lead); writing - original draft (supporting); writing - review and editing (supporting).

DATA AVAILABILITY STATEMENT

The data supporting the findings of this study will be deposited in the Data Repository at the University of Minnesota (DRUM) following acceptance of this paper. An update to this data availability statement, including a DOI for the DRUM repository, will be provided in the proofs.

REFERENCES

- ¹L. Miller, K. Soulliere, S. Sawyer-Beaulieu, S. Tseng, and E. Tam, Materials **7**, 5883–5902 (2014).
- ²A. Tullo, Chem. Eng. News **94**, 32–37 (2016).
- 3 "The New Plastics Economy Rethinking the future of plastics," Tech. Rep. (World Economic Forum, Ellen MacArthur Foundation, and McKinsey & Company, 2016).
- ⁴ "Advancing Sustainable Materials Management: 2018 Fact Sheet," Tech. Rep. (U.S. E.P.A., 2020).
- $^5\mathrm{J.-P.}$ Lange, ACS Sustainable Chemistry & Engineering 9, 15722–15738 (2021).
- ⁶P. J. Flory, *Principles of Polymer Chemistry* (Cornell Univ. Press, 1953).
- $^7\mathrm{D.}$ Nwabunma and T. Kyu, eds., Polyolefin Blends (Wiley, 2007).
- ⁸J. M. Eagan, J. Xu, R. Di Girolamo, C. M. Thurber, C. W. Macosko, A. M. LaPointe, F. S. Bates, and G. W. Coates, Science **355**, 814–816 (2017).
- ⁹J. Xu, J. M. Eagan, S.-S. Kim, S. Pan, B. Lee, K. Klimovica, K. Jin, T.-W. Lin, M. J. Howard, C. J. Ellison, A. M. LaPointe, G. W. Coates, and F. S. Bates, Macromolecules **51**, 8585–8596 (2018).
- $^{10}\mathrm{W}.$ M. Barentsen and D. Heikens, Polymer 14, 579–583 (1973).
- ¹¹O. F. Noel III and J. F. Carley, Polym. Eng. Sci. **15**, 117–126 (1975).
- $^{12}\mathrm{J}.$ Noolandi and K. M. Hong, Macromolecules $\mathbf{15},\;482\text{--}492$ (1982).
- $^{13}\mathrm{J}.$ Noolandi and K. M. Hong, Macromolecules $\boldsymbol{17},$ 1531–1537 (1984).
- $^{14}\mathrm{L}.$ Leibler, Makromol. Chem. 16, 1–17 (1988).

PLEASE CITE THIS ARTICLE AS DOI: 10.1063/5.0170650

- ¹⁵K. R. Shull, E. J. Kramer, G. Hadziioannou, and W. Tang, Macromolecules **23**, 4780–4787 (1990).
- ¹⁶L. Leibler, Physica A, 258–268 (1991).
- $^{17}\mathrm{K}.$ Chang, C. W. Macosko, and D. C. Morse, Macromolecules $\mathbf{48},\,8154-8168$ (2015).
- ¹⁸B. D. Favis, Journal of Applied Polymer Science **39**, 285–300 (1990).
- ¹⁹A. P. Plochocki, S. S. Dagli, and R. D. Andrews, Polym. Eng. Sci. **30**, 741–752 (1990).
- ²⁰L. A. Utracki and Z. H. Shi, Polym. Eng. Sci. **32**, 1824–1833 (1992).
- ²¹D. Gersappe, P. K. Harm, D. Irvine, and A. C. Balazs, Macromolecules **27**, 720–724 (1994).
- ²²E. A. Eastwood and M. D. Dadmun, Macromolecules **35**, 5069–5077 (2002).
- ²³K. R. Shull, Macromolecules **35**, 8631–8639 (2002).
- ²⁴M. D. Lefebvre, C. M. Dettmer, R. L. McSwain, C. Xu, J. R. Davila, R. J. Composto, S. T. Nguyen, and K. R. Shull, Macromolecules 38, 10494–10502 (2005).
- ²⁵H.-J. Qian, Z.-Y. Lu, L.-J. Chen, Z.-S. Li, and C.-C. Sun, J. Chem. Phys. **122**, 184907 (2005).
- ²⁶K. Chang, C. W. Macosko, and D. C. Morse, Macromolecules **40**, 3819–3830 (2007).
- ²⁷J. H. Ryu, Y. Kim, and W. B. Lee, Physical Review E **97**, 042502 (2018).
- ²⁸K. Klimovica, S. Pan, T.-W. Lin, X. Peng, C. J. Ellison, A. M. LaPointe, F. S. Bates, and G. W. Coates, ACS Macro Lett. **9**, 1161–1166 (2020).
- ²⁹J. L. Self, A. J. Zervoudakis, X. Peng, W. R. Lenart, C. W. Macosko, and C. J. Ellison, JACS Au 2, 310–321 (2022).
- $^{30}\mathrm{J}.$ A. Mysona, A. V. McCormick, and D. C. Morse, Physical Review E $\mathbf{102},\,022605$ (2020).
- ³¹K. Nomura, X. Peng, H. Kim, K. Jin, H. J. Kim, A. F. Bratton, C. R. Bond, A. E. Broman, K. M. Miller, and C. J. Ellison, ACS Applied Materials & Interfaces 12, 9726–9735 (2020).
- ³²K. Kremer and G. S. Grest, J. Chem. Phys. **92**, 5057–5086 (1990).
- ³³G. S. Grest, M.-D. Lacasse, K. Kremer, and A. M. Gupta, J. Chem. Phys. **105**, 10583–10594 (1996).
- ³⁴J. D. Weeks, D. Chandler, and H. C. Andersen, J. Chem. Phys. **54**, 5237–5247 (1971).
- $^{35}\mathrm{T.}$ E. I. Gartner and A. Jayaraman, Macromolecules $\mathbf{52},\,755-786$ (2019).
- ³⁶R. Auhl, R. Everaers, G. S. Grest, K. Kremer, and S. J. Plimpton, J. Chem. Phys. 119, 12718–12728 (2003).
- ³⁷J. A. Anderson, J. Glaser, and S. C. Glotzer, Comput. Mater. Sci. **173**, 109363 (2020).

PLEASE CITE THIS ARTICLE AS DOI: 10.1063/5.0170650

- ³⁸C. S. Adorf, P. M. Dodd, V. Ramasubramani, and S. C. Glotzer, Comput. Mater. Sci. 146, 220–229 (2018).
- $^{39} \rm{J.}$ G. Kirkwood and F. P. Buff, J. Chem. Phys. ${\bf 17},\,338–343$ (2004).
- ⁴⁰J.-C. Neyt, A. Wender, V. Lachet, A. Ghoufi, and P. Malfreyt, Journal of Chemical Theory and Computation **10**, 1887–1899 (2014).
- ⁴¹J. Noolandi, Die Makromol. Chem., Theory and Simulations 1, 295–298 (1992).
- ⁴²V. Ramasubramani, B. D. Dice, E. S. Harper, M. P. Spellings, J. A. Anderson, and S. C. Glotzer, Comput. Phys. Comm. **254**, 107275 (2020).
- ⁴³U. Jorzik and B. A. Wolf, Macromolecules **30**, 4713–4718 (1997).
- ⁴⁴Y. Deng, H. Sun, X. Hu, K. Wang, C. Long, F. Yu, and Z.-R. Chen, Macromolecules **56**, 5754–5764 (2023).